26 -06- 2010

תכנית-מחקר המוגשת לאישור כתכנית לעבודת-דוקטור

מערכות דימות מתקדמות ויישומן בהנדסת רקמות שלד המבוססת על תאי גזע

Multi Modality Functional Molecular & Micro Imaging for Stem Cell Based Skeletal Tissue Regeneration

שם התלמיד: **אילן קלאי**
Ilan Kallai

שמות המדריכים: **פרופ' דן גזית, ד"ר גדי פלד**
הפקולטה לרפואת שיניים
האוניברסיטה העברית בירושלים

תאריך הגשת ההצעה: 28.6.2010

"הריני מאשר את הנושא ואת התוכנית, ומסכים להדריך את המועמד/ת בביצוע עבודה זו".

פרופ' דן גזית _____

ד"ר גדי פלד _____

General Introduction:

The need for new strategies for tissue regeneration has led to the emergence of a new field: tissue engineering. Here cells, bioactive factors and biodegradable matrices are combined for use in the replacement of damaged tissues or organs. Mesenchymal stem cells (MSCs) can differentiate into the osteogenic, adipogenic, chondrogenic and tenogenic lineages, and therefore are promising candidates for skeletal tissue regeneration[1]. However much has to be learned of the fate and function of these cells in the living tissue. Advanced molecular and micro imaging methods play an increasingly important role in the rigorous evaluation of stem cell-based tissue regenerative strategies. Imaging techniques such as high-resolution micro-computed tomography (microCT) and optical (bioluminescence and fluorescence) imaging provide non-invasive, real-time, quantitative tools for cell and tissue analysis.

The major aim of this proposed research plan is to investigate the application of various quantitative imaging techniques for the analysis of stem cell-based skeletal tissue regeneration. This proposal is divided into the following four chapters:

1. ***MicroCT Structural Analysis of Various Bone Tissue Regeneration Models:*** The objective of this chapter is to establish specific protocols for regenerated bone scanning and analysis using a Desktop Cone-Beam MicroCT 40 system. Micro–computed tomography (microCT) analysis is a powerful tool for the evaluation of bone tissue because it provides access to its three-dimensional (3D) microarchitecture. The quantitative assessment of macrostructural characteristics, such as geometry, and microstructural features, including relative mineralized bone volume, bone thickness, and connectivity, may improve our ability to evaluate the quality of newly formed bone. Several research models of bone regeneration have been reported. For each model of regeneration I have developed a unique procedure for the evaluation of bone structure and repair. Precise protocols are crucial in this type of analysis, because the system is extremely user-sensitive and results can be easily biased if standard methods are not applied. ***(pages 3-7)***

2. ***Novel Fluorescence Molecular Tomography (FMT) and Applications in Stem Cell–Based Bone Tissue Engineering:*** Although microCT-based bone imaging provides high resolution analysis of bone tissue, it cannot be used frequently on living subjects due to the negative effect of x-rays on cells. Yet fluorescence imaging is a sensitive safe method that can be used to monitor cellular and tissue processes if the right probe and imaging system exist. In this chapter the hypothesis is that engineered bone remodeling can be non-invasively and quantitatively monitored in 3D using FMT and the Osteosense reagent. In order to pursue this hypothesis we longitudinally analyze bone formation in vivo using a novel noninvasive, real-time, and quantitative near infrared (NIR)

imaging technology combined with microCT analysis. This study indicates that newly formed bone binds the fluorescent disphosphonate imaging agent in both nonosteogenic and fracture sites to yield a detectable and quantifiable NIR fluorescent signal. The results of this study show for the first time functional imaging of the processes underlying bone formation with optical tomography in vivo and in real time. These findings demonstrate the effectiveness of FMT as a functional method for molecular imaging in the field of bone regeneration and tissue engineering. ***(pages 8-13)***

3. ***Advanced Imaging-Based Biomechanical Analysis of Bone Regeneration:*** We have previously shown that BMP-2 engineered MSCs can induce non-union fracture repair in a radius bone defect model, showing prominent new bone formation. However, the structural and biomechanical properties of the regenerated bone after a prolonged period of time remained unknown. In this study the hypothesis is that the new bone tissue formed by BMP-engineered MSCs in a critical-size bone defect, remodels and provides biomechanical competence over time. In order to investigate this hypothesis, finite element models and microCT-based imaging are being used for the analysis and quantification of biomechanical and structural changes of regenerated bone. The results show that the regenerated bone tissue remodels over time, as indicated by a significant decrease in bone volume, total volume and connectivity density combined with an increase in mineral density. In addition, the axial stiffness of limbs repaired with MSCs was 2 to 1.5 times higher compared to the contralateral intact limbs, at 10 and 35 weeks post treatment. In conclusion, although MSCs induce bone formation, which exceeds the fracture site, significant remodeling of the repair callus occurs over time. In addition, limbs treated with an MSC graft demonstrate superior biomechanical properties, which could indicate the clinical benefit of future MSC application in nonunion fracture repair. ***(pages 14-18)***

4. ***Molecular and Tissue Imaging for Stem Cell Therapeutics of Vertebral Fracture:*** In this chapter the hypothesis is that the minimally invasive injection of MSCs with a biocompatible scaffold, into the vertebral body will regenerate the spinal vertebral body and accelerate bone repair. The objective of this study is to monitor stem cell-based vertebral fracture repair using molecular and tissue imaging modalities. In order to achieve this objective, MSCs with a biocompatible scaffold will be implanted into the fractured vertebral body of a rat model. Monitoring of cell survival and bone formation kinetics is based on optical (bioluminescence and fluorescence) molecular and micro imaging. Additional studies will determine optimal cell scaffold compositions that would yield the desired osteogenic effect. ***(pages 19-24)***

Chapter 1: MicroCT Structural Analysis of Various Bone Tissue Regeneration Models

Abstract:

Micro–computed tomography (microCT) analysis is a powerful tool for the evaluation of bone tissue because it provides access to the three-dimensional (3D) microarchitecture of bone. It is invaluable for regenerative medicine since it provides the researcher with the opportunity to explore the skeletal system both *in vivo* and *ex vivo*. The quantitative assessment of macrostructural characteristics, such as geometry, and microstructural features, including relative mineralized bone volume, bone thickness, and connectivity, may improve our ability to estimate the quality of newly formed bone. Several research models of bone regeneration have been reported. For each model of regeneration we have developed a unique procedure for the evaluation of bone structure and repair. Precise protocols are crucial in this type of analysis, because the system is extremely user-sensitive and results can be easily biased if standard methods are not applied.

***Introduction*:**

Tissue engineering is a rapidly growing field designed to provide biological replacement therapies for damaged tissues and organs. Previously we demonstrated success in the use of mesenchymal stem cells, multi-potent adult stem cells, for skeletal tissue regeneration, including that of bone[1].

Advanced micro-imaging methods play an increasingly important role in the rigorous evaluation of tissue regeneration strategies. Micro–computed tomography (MicroCT) is an x-ray–based imaging method that provides easy and relatively inexpensive access to the three-dimensional (3D) microarchitecture of bone. This imaging modality is based on a micro-focus x-ray source that illuminates the object and a planar detector that collects magnified projection images. Hundreds of angular views are acquired while the object of interest rotates. From these views a computer synthesizes a stack of virtual cross sections, interpolating sections along different planes, to inspect the internal structure of the object. Based on these data the computer can reconstruct a realistic 3D image and cut it into slices to produce 2D images[2]. A quantitative 3D histomorphometric evaluation can then be performed on a cubic volume or an irregularly shaped volume of interest (VOI). The VOI is defined by a set of free hand contours or by geometric objects such as rectangles or ellipses. The VOI must be drawn using a slice-based method.

MicroCT is an invaluable tool for skeletal regenerative medicine because it provides the researcher with the opportunity to explore the skeletal system both *in vivo* and *ex vivo*. The quantitative assessment of bone's macrostructural characteristics, such as geometry, and its

microstructural features, such as relative mineralized bone volume, bone thickness, and connectivity, may improve our ability to estimate the quality of regenerated bone.

We have published several studies featuring bone-tissue regeneration models in which microCT analysis played a major role in the evaluation of results [3, 4, 5, 6]. **The objective of this chapter is to establish a protocol of detailed microCT analysis procedures for various bone regeneration models.**

***Methods*:**

In developing our microCT analysis procedures, we tested three main models of bone-tissue regeneration, the experimental designs for which have been described elsewhere (see references for each model). These three types are:

1. *Ectopic bone formation model* — In this model bone formation is induced in a location where it is not normally expected to occur. Our ectopic model includes two subtypes: intramuscular [4, 5, 6, 7] and subcutaneous [3, 8] bone formations.
2. *Segmental defect in a long-bone model* — In this model a fracture is created in a long bone by removing a fragment of the bone. Using this model we induce nonunion fracture repair in a mouse radial defect [3, 6, 7, 9].
3. *Round critical-size bone defect model* — In this model a bone void is created by drilling through the bone. This model is used for mandible defect regeneration [5] and calvarial defect regeneration [10].

Bone formation in the sites of regeneration was evaluated using microCT analyses. In addition to the visual assessment of structural images provided by this technology, morphometric indices can be determined on the basis of microtomographic data sets by using direct 3D morphometry[3]. To quantify bone regeneration and compare it between several samples, a standard method must be used. The principles of our protocol primarily focus on the standardization of the samples and the proper selection and adjustments of the VOI for the quantitative analysis. These procedural steps have a great effect on the outcomes of the analysis. Precise protocols are crucial in this type of analysis, because the system is extremely user-sensitive and results can be easily biased if standard methods are not applied.

This protocol was designed for use with a Desktop Cone-Beam MicroCT Scanner (μCT 40; SCANCO Medical AG, Brüttisellen, Switzerland). The evaluation of 3D scanned data was handled by the software provided with the scanner: IPL (Image Processing Language), an advanced script-

based 3D-volume analysis tool. In this protocol we describe evaluation procedures conducted using SCANCO's software. Adjustments will be needed if other company's software is used.

Results:

Figure 1.1, as published by Kimelman-Bleich et al. (2009), shows microCT analysis of ectopic bone formation. The hypothesis of that study was that an oxygen-enriched hydrogel scaffold (supplemented with PFTBA) would enhance tissue-engineered bone formation in vivo, using mouse MSCs that overexpress the recombinant human bone morphogenetic protein–2 (rhBMP2) under tetracycline regulation, denoted as mMSCs-rhBMP2. When ectopic bone formation was analyzed, we noticed a significant increase in bone volume in the PFTBA groups compared with the no PFTBA controls. Other morphometric indices, such as bone mineral density, were not significantly different between groups, indicating that only bone quantity was affected by PFTBA supplementation in this study.

***Figure 1.1*: MicroCT analysis of ectopic bone formation model.**
Effect of PFTBA on ectopic bone formation. One million mMSCs-rhBMP2 were suspended in fibrin gel supplemented with 5 or 10% PFTBA or in gel with no PFTBA. Two weeks after subcutaneous implantation, the cell–gel implants were harvested and bone formation was analyzed using microCT. a) Bone volume analysis. Note that supplementation with 10% PFTBA (n=15 implants) enhanced bone formation significantly (*$p < 0.05$) compared with the no PFTBA group (n=16 implants). b) Representative images of newly formed bone from ectopic sites (bar = 1 mm).

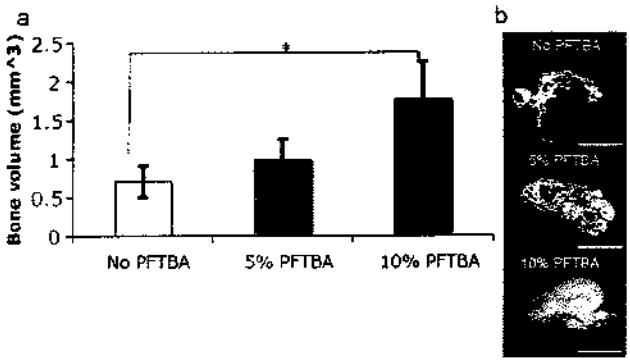

Figure 1.2, as published by Tai et al. (2008), shows microCT analysis of radial nonunion fracture repair model. MicroCT three-dimensional images indicated substantial growth of engineered bone, indicative of fracture healing at the transplantation site (Fig.1.2 b). Two-dimensional images demonstrated that the new bone tissue was composed of distinct cortical-like and trabecular-like regions (Fig.1.2 b), as indicated by the degree of porosity on the outer rim and the inner region, respectively. Quantitative morphological and structural analysis of the bone tissue indicated that the morphology of engineered bones is significantly different from native intact bones.

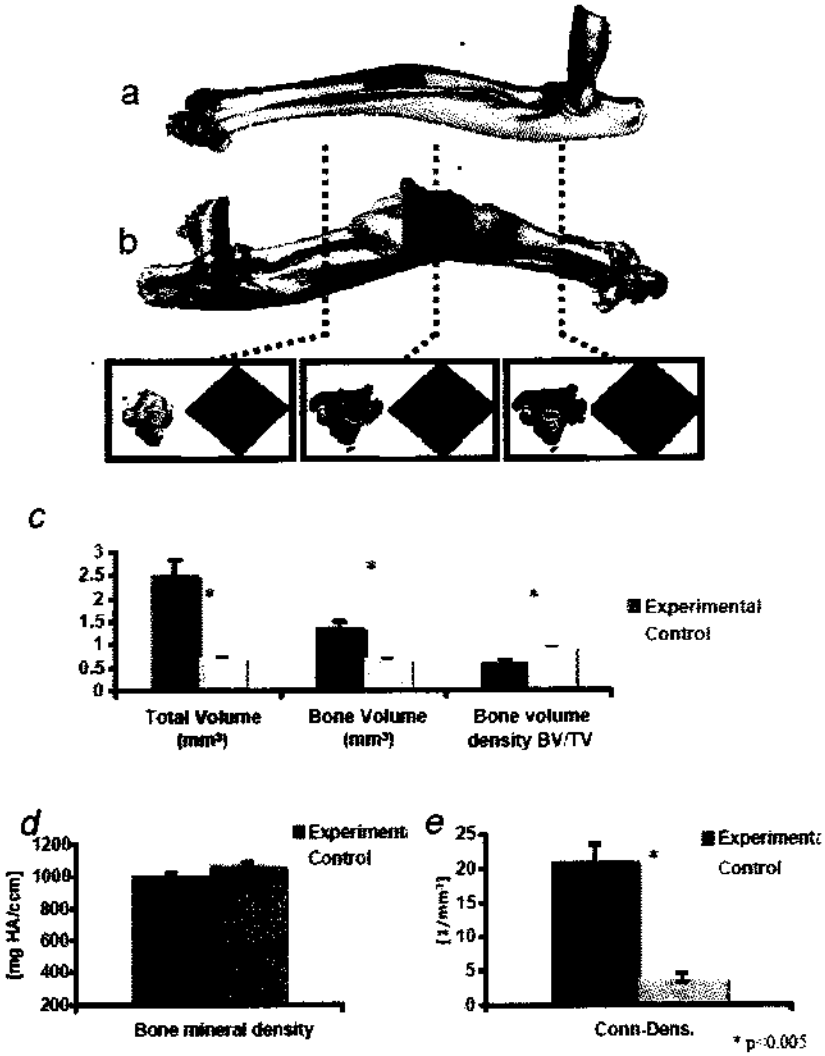

***Figure 1.2*: MicroCT analysis of radial nonunion fracture repair model.**
3D microCT images of (a) native radius and (b) a radial defect regenerated with engineered bone, Eight weeks post implantation of mMSCs-rhBMP2 into the radial defect. Images obtained by microCT demonstrated the formation of new bone tissue within the implantation site. The orange-highlighted region represents the regions in the intact and repaired radii that were quantitatively analyzed. The bone volume density was calculated as the ratio of actual bone volume to total tissue volume (c). Bone mineral density indicates the mineral content of the bone tissue (d). The parameter of connectivity density describes the porosity of the bone sample and quantifies the degree of branching in the bone tissue structure (e). Bars indicate standard error. The asterisk (*) pairs indicate a statistical difference with $p<0.05$

Figure 1.3, as published by Steinhardt et al. (2008), shows microCT analysis of mandibular defect regeneration. This analysis demonstrated that MSC-hBMP2 induced new bone formation and led to 84% healing of the defects (Fig.1.3 a). Partial regeneration (51–53%) of the defect was observed in the control groups, but a significant enhancement in bone regeneration was observed in the MSC-hBMP2 group in microCT scans (Fig.1.3 b, c). Moreover, mice implanted with MSC-lacZ and mice without any implant showed little bone formation or defect regeneration (Fig.1.3 a), indicating that implantation of non-engineered MSCs in the mandibular defect did not promote regeneration.

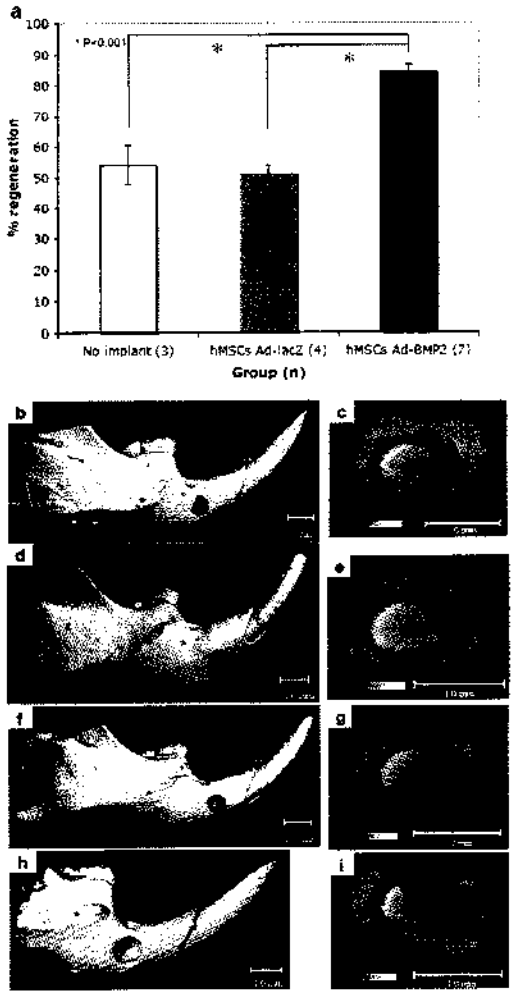

***Figure 1.3*: microCT analysis of mandibular defect regeneration.**
Defect regeneration in control groups (white and gray bars) and in the BMP2-treated group (black bar) (a). MicroCT 3D reconstruction images (b, d, f, h) and 2D coronal images (c, e, g, i) showing extent of bone regeneration in defects that received MSC-hBMP2 (b, c), MSC-lacZ (d, e), or no implant (f, g). Defect site is marked in orange. Panels (h) and (i) depict the defect before cell implantation.

***Discussion and future plans*:**

MicroCT analysis is a powerful tool for the evaluation of bone tissue regeneration models. For each model of regeneration I have developed a unique protocol for structural and repair evaluation. Precise protocols are crucial in this type of analysis because the system is extremely user-sensitive, and results can be easily biased if standard methods are not applied.

My goal in this chapter is to establish a protocol of detailed microCT analysis procedures for various bone regeneration models. I have already established the protocols for ectopic bone formation, radial nonunion fracture repair, mandibular defect regeneration and calvarial defect regeneration. Next, a protocol will be established for a vertebral fracture repair model (see chapter 4).

A manuscript will be submitted to "Nature. Protocols". This manuscript will include detailed microCT analysis procedures for various bone regeneration models. I believe that the principals introduced in this protocol are of significant value to investigators in the field of bone tissue engineering and can be easily modified for a variety of bone tissue regeneration models.

Chapter 2: Novel Fluorescence Molecular Tomography (FMT) and Applications in Stem Cell–Based Bone Tissue Engineering

Abstract:

Fluorescence molecular tomography (FMT) is a novel tomographic near-infrared (NIR) imaging modality that enables 3D quantitative determination of fluorochrome distribution in tissues of live small animals at any depth. This study demonstrates a noninvasive, quantitative method of monitoring engineered bone remodeling via FMT.

Murine mesenchymal stem cells overexpressing the osteogenic gene *BMP2* (mMSCs-BMP2) were implanted into the thigh muscle and into a radial nonunion bone defect model in C3H/HeN mice. Real-time imaging of bone formation process was performed following systemic administration of the fluorescent bisphosphonate imaging agent OsteoSense^{TM}, an hydroxyapatite (HA)–directed bone-imaging probe. The mice underwent imaging on Days 7, 14, and 21 post-implantation. New bone formation at the implantation sites was quantified using micro–computed tomography (microCT) imaging.

The results demonstrated a higher fluorescent signal at the site of the mMSC-BMP2 implants than that found in controls. MicroCT imaging revealed a mass of matured bone formed in the implantation sites on Day 21–a finding also confirmed by histology.

In-vivo bone formation process has been demonstrated quantitatively using noninvasive, real-time, 3D molecular optical imaging with NIR light. These findings highlight the effectiveness of FMT as a functional platform for molecular imaging in the field of bone regeneration and tissue engineering.

***Introduction*:**

Optical imaging of live animals has become an important tool in biomedical research as advances in photonic technology and reporter strategies have led to widespread exploration of biological processes *in vivo*. *In vivo* optical imaging has traditionally been limited to planar or reflectance approaches, which produce 2D fluorescence images of the target tissue with appropriate spectral filters. Planar imaging has low penetration depths (< 1 cm) and cannot quantify fluorescence or provide depth or size information. Fluorescence molecular tomography (FMT) imaging is a novel modality used for localization and quantification of fluorescent probes in tissues, especially when compared with single-view or planar imaging techniques.[7] FMT optically quantifies fluorescence by resolving the ambiguity afflicting planar imagers about depth, size, and concentration. The system exploits 50,000 to 100,000 source-detector pair measurements to invert a diffusion model of photon propagation in turbid media.[8] By normalizing every fluorescence measurement with its

corresponding source-detector pair excitation measurement, FMT can handle the optical heterogeneity of biological tissue robustly and is thus able to resolve the aforementioned ambiguity. FMT reconstruction of fluorescence provides a depth-uniform three-dimensional fluorochrome distribution with sub-millimeter resolution.[9]

Development and maintenance of the vertebral skeleton depends on a balance between osteoblast and osteoclast activity. Changes in this balance are characteristic of numerous disease states, including arthritis, osteoporosis, and cancer metastases. Hydroxyapatite (HA) is the major mineral product of osteoblasts and is a good biological marker for osteoblast activity, which is indicative of many different disease states. HA binds to pyrophosphonates and phosphonates as well as to synthetic bisphosphonates with high affinity. In fact, bisphosphonates are widely prescribed for a broad range of clinical indications including osteoporosis and bone complications arising from malignancies. Radiolabeled bisphosphonates are also used as clinical imaging agents for bone scans. Based on previous research,[10] we selected for use a near-infrared (NIR) bisphosphonate (pamidronate) imaging agent, OsteoSense, which binds to HA with high affinity *in vitro* and *in vivo*. OsteoSense is able to rapidly image bone growth and remodeling with a high sensitivity and resolution and no need for radioisotopes.

We have previously described a stem cell-based strategy for bone regeneration, in which mesenchymal stem cells (MSCs) are ex-vivo genetically modified to express an osteogenic gene, and implanted in critical-size bone defects.[11] A murine model system was established to test bone repair of nonunion fractures with the aid of MSCs overexpressing recombinant human bone morphogenetic protein–2 (rhBMP2).[12] RhBMP2 is a highly potent osteoinductive protein that induces bone formation in vivo[13-15] and osteogenic differentiation in vitro.[16-24] BMP2 induces differentiation of stem cells into osteoblastic and chondroblastic cells in vitro.[11, 19, 25-27] As a result, MSCs overexpressing BMP2 have an enhanced therapeutic effect in healing bone-segment defects through a dual mechanism: the paracrine mechanism, in which rhBMP2 exerts an effect on host stem cells, and the autocrine mechanism, in which rhBMP2 induces the osteogenic differentiation of the transplanted stem cells themselves.[11]

The hypothesis of this chapter is that engineered bone remodeling could be non-invasively and quantitatively monitored in 3D using FMT and the Osteosense reagent. The use of novel micro imaging systems in skeletal research could provide better insight to the mechanisms underling skeletal disorders and promote novel therapeutics such as stem cell-based tissue engineering.

Specific Aim:

- Longitudinally analyze bone formation induced by the implantation of genetically modified MSCs using a novel noninvasive, real-time, quantitative NIR imaging technology combined with micro-CT analysis.

***Methods*:**

mMSCs-rhBMP2 were implanted in the thigh muscle and radius non-union bone defect sites in C_3H/HeN mice. 2×10^6 mMSCs-rhBMP2 cells in 100 µl PBS were injected into the right hind thigh muscle of the mouse, via the calf muscle. In the control mice group, 2×10^6 C3H/LacZ cells in 100 µl PBS were injected in the same procedure. 2×10^6 mMSCs-rhBMP2 cells in 30 µl PBS were loaded on standard 1x3 mm DuraGen sponge (Integra LifeSciences Corporation) and were transplanted into 2.5-mm segmental defects created in the radii of the same group of injected thigh muscle mice. The Control mice group was not operated and served as baseline of bone remodeling process in the normal non-damaged radius bone.

Real time imaging of bone remodeling was performed after systemic administration of the fluorescent diphosphonate imaging agent, OsteoSense™ on Day 7, 14 and 21 post-implantation using VisEn's FMT™ Fluorescence Molecular Tomography system. In addition, we monitored and quantified bone formation in the implantation sites using micro-CT on Day 21.

***Results*:**

The FMT images and tomographic reconstructions showing ectopic bone growth in the thigh muscle and nonunion fracture healing in the radius provided a clear visualization and quantification of new bone formation over time as well as bone healing in the nonunion fracture site.

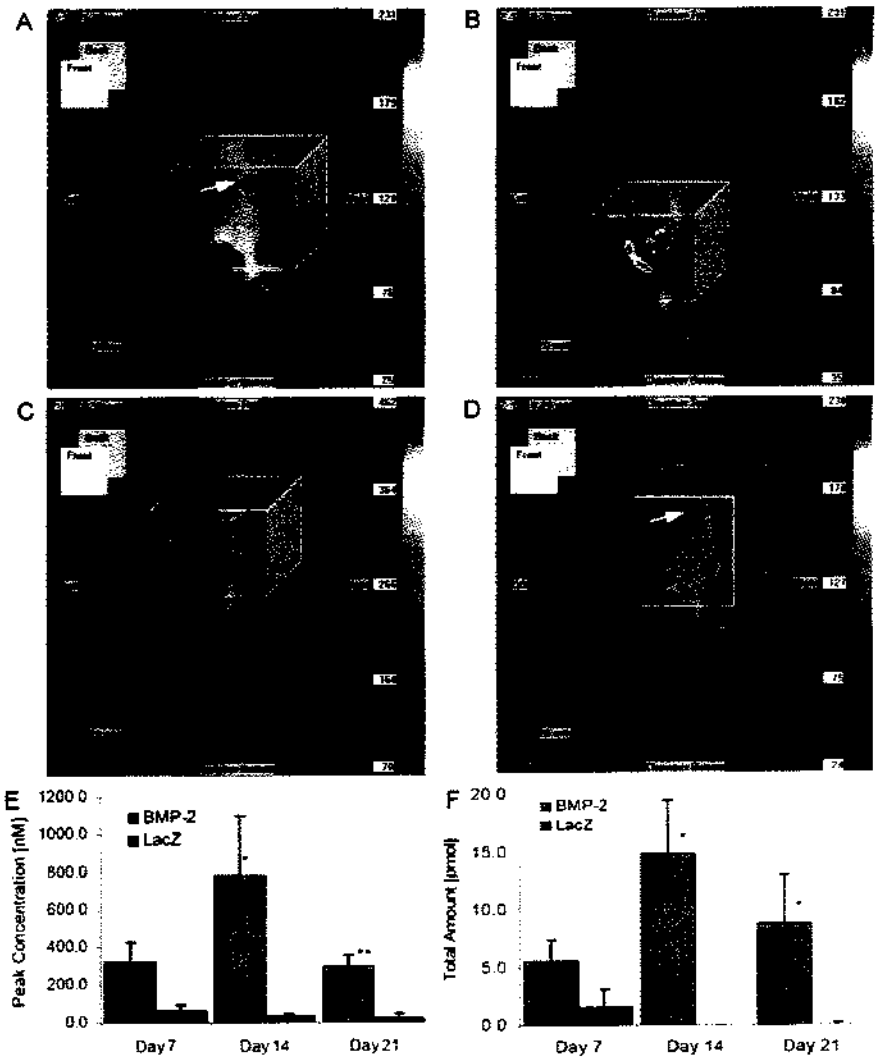

Figure 2.1: Ectopic bone formation. FMT images obtained 1, 2, and 3 weeks after injection of mMSCs-rhBMP2 cells (A-C) compared with control C3H/LacZ cells (D) at 2 weeks. The signals from the knee (white arrow) indicate continual bone erosion and growth. Fluorescence quantification data from the FMT reconstructions obtained on Days 7, 14, and 21 (E & F) as peak fluorescence (nM, mean ± SEM) and the total amount of fluorescence (pmol, mean ± SEM; n = 4-7 mice per group). Asterisks represent statistically significant differences (*$p < 0.05$, **$p < 0.01$) compared with C3H/LacZ control as determined by the Student *t*-test.

Figure 2.1 A–D shows representative sagittal images obtained at a discrete depth (2 mm) registered onto a grayscale anatomical registration image of the hind limb. Although little or no signal could be detected in control mice that had been injected with cells expressing LacZ (Fig. 2.1 D), the thighs of mice injected with BMP2-expressing cells displayed a significant OsteoSense™ fluorescent signal (Fig. 2.1 A–C). Three-dimensional ROIs were drawn around the thigh muscle regions. The peak concentration of the fluorochrome (in nanomoles per liter) and its total amount (in picomoles) were automatically calculated relative to standards generated with known concentrations of appropriate dyes. Both the peak concentration (Fig. 2.1 E) and the total amount (Fig. 2.1 F) of fluorochrome were significantly higher in experimental mice than in control mice on Days 14 and 21 ($p = 0.0425$ and 0.0036 for the peak concentration and $p = 0.0125$ and 0.0468 for the total amount of fluorochrome for Days 14 and 21, respectively). These findings indicate that new bone in the thighs of experimental mice binds OsteoSense to yield a detectable and quantifiable near-infrared fluorescence (NIRF) signal.

Figure 2.2 A–D shows representative sagittal images registered onto a grayscale anatomical registration image of the forelimb. Again, little or no signal could be detected in control mice that had been transplanted with cells expressing LacZ (Fig. 2.2 D), the limbs of mice injected with BMP2-expressing cells displayed a significant OsteoSense™ fluorescent signal on day 21 (Fig. 2.2 C). On Day 21, the total amount of fluorescence, but not its peak concentration, was significantly higher in the radii of mice with nonunion fractures implanted with mMSCs-rhBMP2, compared with the radii of control mice implanted with MSCs expressing LacZ ($p = 0.0045$) (Fig. 2.2 F).

Micro-CT analysis revealed a large mass of matured bone formed in the thigh muscle and in the radius segmental defect on day 21, confirmed by Histology H&E.

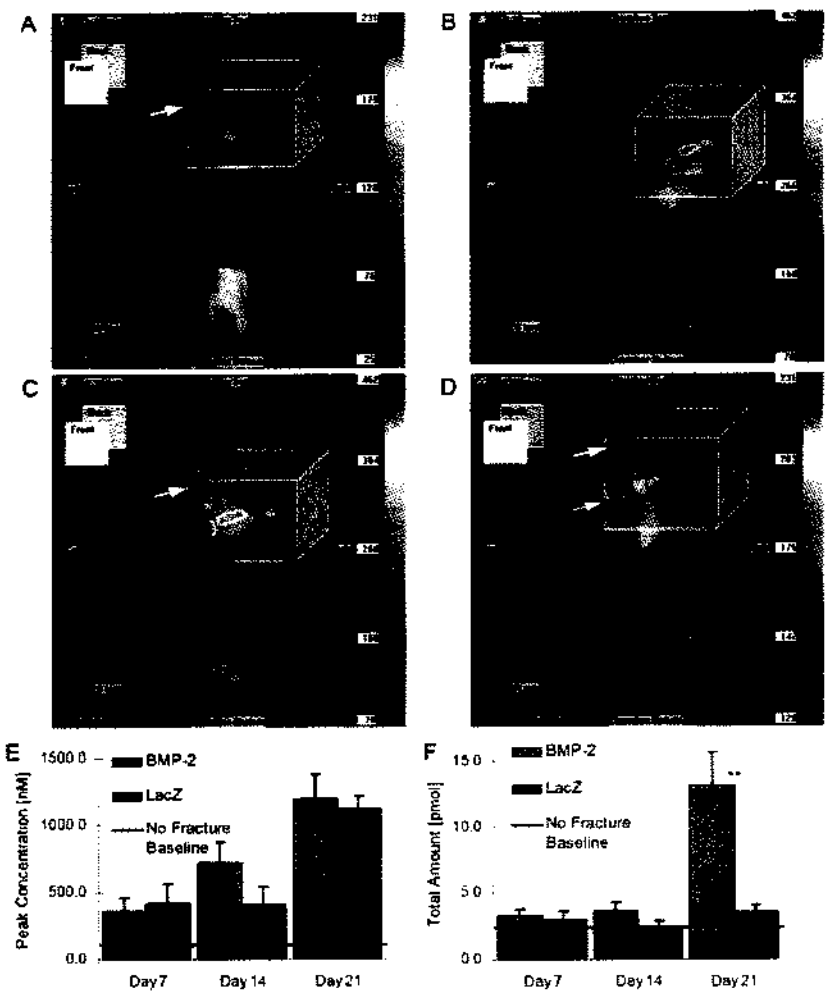

Figure 2.2: Radial nonunion defect. FMT images obtained 1, 2, and 3 weeks after implantation of mMSCs-rhBMP2 cells (A-C) compared with control C3H/LacZ cells (D) at 3 weeks. The signals from the elbow (yellow arrow) and shoulder (white arrow) joints indicate continual bone erosion and growth. Fluorescence quantification data from the FMT reconstructions obtained on Days 7, 14, and 21 (E & F) as peak fluorescence (nM, mean ± SEM) and total amount of fluorescence (pmol, mean ± SEM; n = 4-7 mice per group). Asterisks represent statistically significant differences (**$p < 0.01$) compared with control (C3H/LacZ cells) as determined by the Student *t*-test.

***Discussion and future plans*:**

This study indicates that newly formed bone binds the fluorescent disphosphonate imaging agent in both nonosteogenic and fracture sites to yield a detectable and quantifiable NIRF signal, showing

for the first time functional imaging of the processes underlying bone formation with optical tomography in vivo and in real time. The use of tomographic methods can transform macroscopic optical observations of tissues from a crude qualitative tool to an accurate 3D imaging technique. The combination of optical and micro-CT imaging modalities with complementary features offers an attractive future direction for study. Correlation of micro-CT and FMT data revealed that the process of bone remodeling was almost completed during a 21-day period. This is the first report that demonstrates the feasibility of non-invasive, 3D, real-time, molecular imaging of the in vivo bone formation process. These findings demonstrate the effectiveness of FMT as a functional platform for molecular imaging in the field of bone regeneration and tissue engineering.

Results of this study were published in the Journal of Orthopaedic Research [28].

Future studies will utilize Optoacoustic (or photoacoustic) tomography, a hybrid non-invasive imaging modality that has recently demonstrated high-resolution 3D visualization of molecular probes located deep in scattering living tissues of small animals that was not available until now. This imaging method relies on detection of ultrasonic signals induced by absorption of pulsed light. We wish to be the first to utilize optoacoustic tomography in a bone regeneration model in-vivo using Osteosence™ florescent probe.

Chapter 3: Advanced Imaging-Based Biomechanical Analysis for Bone Regeneration

Abstract:

Stem cell-mediated gene therapy for fracture repair, utilizes genetically engineered mesenchymal stem cells (MSCs) for the induction of bone growth and is considered a promising approach in skeletal tissue regeneration. Previous studies have shown that murine nonunion fractures can be repaired by implanting MSCs over-expressing recombinant human bone morphogenetic protein-2 (rhBMP-2). Nanoindentation studies of bone tissue induced by MSCs in a radius fracture site indicated similar elastic modulus compared to intact murine bone, eight weeks post treatment.

In the present study we sought to investigate temporal changes in microarchitecture and biomechanical properties of repaired murine radius bones, following the implantation of MSCs. High resolution micro computed tomography (Micro-CT) was performed 10 and 35 weeks post MSC implantation, followed by micro finite element (Micro-FE) analysis.

The results have shown that the regenerated bone tissue remodels over time, as indicated by a significant decrease in bone volume, total volume and connectivity density combined with an increase in mineral density. In addition, the axial stiffness of limbs repaired with MSCs was 2 to 1.5 times higher compared to the contralateral intact limbs, at 10 and 35 weeks post treatment. These results could be attributed to the fusion that occurred between in the ulna and radius bones. In conclusion, although MSCs induce bone formation, which exceeds the fracture site, significant remodeling of the repair callus occurs over time. In addition, limbs treated with an MSC graft demonstrated superior biomechanical properties, which could indicate the clinical benefit of future MSC application in nonunion fracture repair

***Introduction*:**

The need for bone tissue regeneration is already high and continuously rising, due to the increased life span and improved quality of life. Although bone tissue has regenerative capabilities, in extreme situations in which the extent of bone loss or damage due to trauma, surgery, or a metabolic disease such as osteoporosis is too large, complete regeneration will not occur. Therefore, the induction of in vivo bone formation is a major goal in a variety of orthopedic and neurosurgical procedures, such as segmental bone fractures and spinal fusion.

Mesenchymal stem cells (MSCs) are adult stem cell population that reside in bone marrow and can also be isolated from other adult tissues like adipose[29]. We have previously shown that, MSCs, genetically engineered to overexpress a bone morphogenetic protein (BMP) gene, can be utilized to

achieve accelerated bone regeneration in a segmental fracture[11, 12, 27] and spine fusion models[30, 31]. These genetically engineered MSCs have an enhanced therapeutic effect in healing bone segmental defects due to a dual mechanism: a paracrine mechanism by which rhBMP-2 exerts its osteoinductive effects on host cells, and an autocrine mechanism in which rhBMP-2 induces the osteogenic differentiation of the transplanted genetically-engineered stem cells themselves[11].

One of the major outcome measures of bone regeneration is the biomechanical property of the repaired tissue. The present "gold standard" of determining bone strength is a functional, mechanical test. Direct mechanical testing is a straightforward procedure, but is limited by its destructiveness. Therefore, this method is not applicable in vivo, and although it can be used in vitro, a sample can only be tested once, which limits the assessment of direction-dependent failure characteristics. Furthermore, these tests are prone to errors related to boundary artifacts and to the often small size of the specimens, both of which hamper the determination of high-precision measurements[32-34].

Micro–computed tomography (MicroCT) is an X-ray–based microstructural imaging method that allows an easy and relatively inexpensive access to the 3-D microarchitecture of bone, thereby giving us a powerful tool for the exploration of genetically engineered bone formation. Although the inclusion of architectural parameters has strongly improved the prediction of bone stiffness for trabecular bone specimens[35], they only do so in a statistical sense. They cannot be relied on to explain the real physical contribution of the microarchitecture to the mechanical failure behavior of bone. To understand how differences in bone microarchitecture influence bone strength, insight into load transfer through bone architecture is needed. Using microstructural finite element (microFE) models generated directly from computer reconstructions of trabecular bone, it is now possible to perform a "virtual experiment," that is, simulate a mechanical test in great detail and with high precision. These computer models allow calculation of loads at the microstructural or even the tissue level[36, 37] and have been used extensively to determine accurately the apparent mechanical properties of bone specimens. Thanks to recent advances in imaging abilities and computer resources, it is now possible to calculate physiological tissue loading when micro-FE models represent whole bones.

In this study we used mMSCs-rhBMP2 to induce endochondral bone formation in a murine nonunion fracture model for the analysis of bone microarchitecture and to assess the biomechanical competence of the healed bone. We have previously utilized ex vivo nanobiomechanics in order to analyze the intrinsic mechanical properties of new bone formed by engineered MSCs in a similar model[5]. Our results showed that intact radius bone exhibited a statistically similar elastic modulus

values compared to that of the engineered bone, while the hardness was found to be marginally statistically different at 1000 μN and statistically similar at 7000 μN. However, that study did not investigate the biomechanical properties of the repaired limb.

Specific Aims:

- Analyzing bone stiffness using micro-FE and combining it with micro-CT analyses of bone formation to obtain a better understanding of the quality of nonunion fracture repair by engineered MSC implantation.
- Investigating the natural remodeling changes that occur in the regenerated bone over time, utilizing structural analysis based on the micro-CT scans.

Methods:

Segmental defects (2.5mm long) were created in the radii of C3H/HeN female mice. Cultured mMSCs-rhBMP2, derived from C3H10T1/2 MSC line[12], were loaded onto a collagen sponge (DuraGen, Integra LifeSciences Co., NJ, USA). The cell-saturated scaffold was placed in the space created by the microsurgery. The intact contralateral limbs of the same mice were used as controls. The mice forelimbs were scanned using a microCT scanner (μCT40; Scanco Medical AG, Bassersdorf, Switzerland) 10 and 35 weeks after implantation. Morphometric indices were determined for the newly formed bone in the nonunion fracture site, by evaluating the central 2 mm of the bone defect. Micro-FE models of the middle 8mm of the radius and ipsilateral ulna were created. Bone tissue was assumed to be isotropic and constant (E=13.4 GPa). The distal part of each model was fully fixed, whereas the proximal part underwent an axial displacement, resulting in 1% overall strain. The long axis of the bones was carefully aligned to the loading direction. The models were used to calculate the force needed to obtain the prescribed displacement, from which apparent stiffness was derived.

Results:

Prominent formation of new bone tissue was evident in the fracture site (Fig. 3.1). The regenerated bone tissue (Fig.3.1 b-c) demonstrated different morphology compared to the intact control (Fig. 3.1 a). The 2D images display changes in the regenerated bone morphology with time (Fig. 3.1, b vs. c).

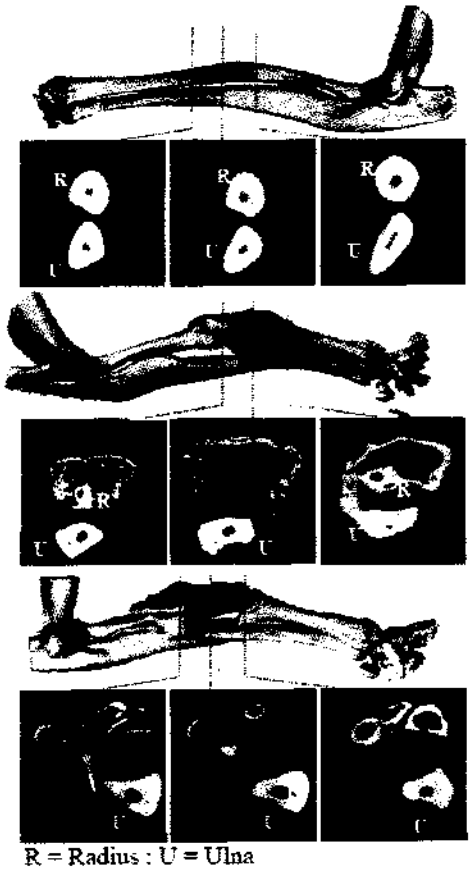

Figure 3.1: MicroCT imaging of intact and regenerated radial bones, 10 and 35 weeks after implantation of collagen sponge loaded with mMSCs-rhBMP2. Cross sections obtained at different locations within the limbs are shown as 2D images. A quantitative analysis of the bone formation in the central 2 mm of the radial defect (marked with orange color) was performed (shown in figure 3.2 a-c).

Quantitative analysis of the newly formed bone in the nonunion fracture site, at 10 vs. 35 weeks after implantation, showed a decrease in bone volume and connectivity density (Fig. 3.2 a-b) and an increase in bone mineral density (Fig. 3.2 c). The structural indices of the regenerated bones, at 35 weeks, were closer to the indices of the intact untreated bones, than the indices at 10 weeks. These changes indicate a remodeling process of the regenerated bone. MicroFE analysis revealed that the regenerated bone was structurally intact. The regenerated bones were substantially stronger than the control ones, having a higher axial stiffness compared to the native bones (Fig. 3.2 d).

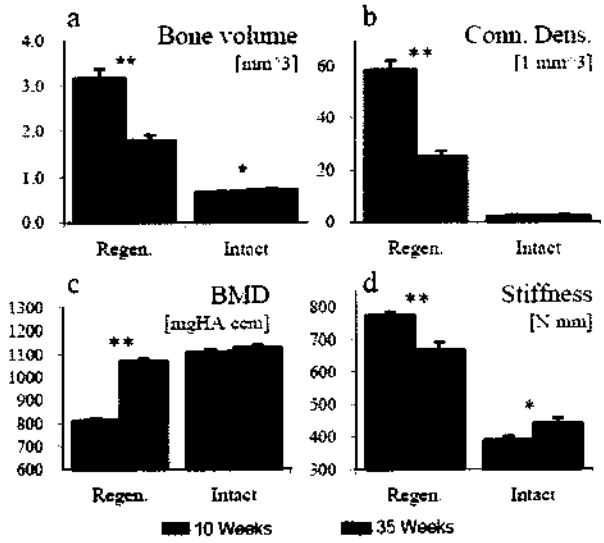

Figure 3.2: Quantitative analysis of the microarchitecture (a-c) and the biomechanics (d) of regenerated and intact radial bones. Statistically significant differences between 10 and 35 weeks are marked (* $p<0.05$; ** $p<0.001$; n=11/group ; two tailed unpaired t-test).

***Discussion and future plans*:**

This study showed that the implantation of BMP-2 over-expressing MSCs in a nonunion bone defect resulted in new bone regeneration, which remodeled over time and provided biomechanical competence to the treated limb. 10 weeks post implantation, the structural indices of the newly formed bone at the fracture site were significantly different ($p < 0.001$) from the intact contralateral radius bones, being composed of a larger mass of thin bone compartments with lower mineral density. At 35 weeks post treatment, the structural indices of the regenerated bones were significantly different than the indices at 10 weeks and closer to the indices of the intact untreated bones.

The axial stiffness of the limbs repaired with engineered MSCs was approximately two times higher than the stiffness of the contralateral intact limbs. Our results showed that the cause for the substantial increase in stiffness of the treated limbs could be found in the high degree of fusion between the radius and the ulna.

Results of this study were published in the Journal of Biomechanics[18].

Further investigations will include:

- *Analyzing potential correlations between the structural changes and the biomechanical properties of the regenerated bone tissue.*
- *Comparisons of ex-vivo and in-vivo microCT evaluations in order to determine the feasibility of the biomechanical analysis in-vivo.*

Chapter 4: Molecular and Tissue Imaging for Stem Cell Therapeutics and Tissue Engineering of Spinal Vertebrae

Abstract:

There is wide prevalence of vertebral compression fractures (VCFs) among osteoporotic patients and the general population. There is a clear clinical need for a biological therapeutic solution that will prevent the deterioration of early collapse in osteoporotic spinal vertebrae, and provide a biological solution to the loss of trabecular and cortical structure of the vertebral body. The hypothesis of this study is that the minimally invasive injection of MSCs with a biocompatible scaffold, into the vertebral body will regenerate the spinal vertebral body and accelerate bone repair. In this chapter the objective is to monitor stem cell-based vertebral fracture repair using molecular and tissue imaging modalities. In order to achieve this objective, MSCs with a biocompatible scaffold are implanted into the fractured vertebral body of a rat model. Monitoring of cell survival and bone formation kinetics is based on optical (bioluminescence and fluorescence) molecular and micro imaging. Additional studies will determine optimal cell scaffold compositions that would yield the desired osteogenic effect.

Introduction:

Vertebral compression fractures (VCFs) are the most common fracture in patients with osteoporosis, affecting about 750,000 people annually. VCFs affect an estimated 25 percent of all postmenopausal women in the United States. Since compression fracture biomechanics are primarily determined by disruption of the trabecular microarchitecture [39] and ongoing symptoms may be related to ineffective structural repair and motion, new, non-biological, methods have been developed to regain the biomechanical properties of the vertebral body. These methods include the minimally invasive procedures of vertebroplasty and balloon tamp reduction (kyphoplasty). Both non-biological procedures involve percutaneous injection of polymethylmethacrylate (PMMA) into the collapsed spinal vertebral body[40, 41]. Unfortunately, these minimally invasive techniques rely on the use of synthetic, non-biological, cement that does not have the physiological properties of natural bone.

Current treatment of osteoporotic patients is mostly focused on prevention of VCFs. However, even new medicines such as alendronate and parathyroid hormone (1-34) have reduced the incidence of new vertebral fractures only by 50 - 65%, respectively[42, 43]. There are a few options of treatment when VCFs occur in osteoporotic patients. Since open surgery involves morbidity and implant failure in this patient population, nonoperative management, including medications and bracing, is usually recommended for the vast majority of patients. Unfortunately, large numbers of

patients report intractable pain and inability to return to activities. The limitations of nonoperative management have fostered increasing interest in new, minimally invasive surgical techniques, such as vertebroplasty and kyphoplasty. Recent study suggests that the prophylatic injection of PMMA into osteoporotic spinal vertebrae better maintains the stiffness of the vertebrae than post fracture injection[44]. However, as indicated above, these are non-biological procedures with subsequent disadvantages and hazards such as pulmonary and cardiac emboli[45-48]. Thus, currently there is no safe biological solution for the treatment of collapsed spinal vertebral body.

There is a clear clinical need for a biological therapeutic solution that will prevent the deterioration of early collapse in osteoporotic spinal vertebrae, and provide a biological solution to the loss of trabecular and cortical structure of the vertebral body.

We have previously shown that the use of adult mesenchymal stem cells (MSCs), induced rapid bone regeneration and fracture repair in various bone loss models, in vivo[12, 27, 30]. In addition, we have established the use of an electroporation-based method for loading MSCs with bioactive molecules[49] that subsequently induce the desired differentiation pattern of the cells, leading to accelerated tissue regeneration. An important factor in tissue engineering is the scaffold in which the cells are delivered to the site of tissue loss. Our recent studies indicated that the enrichment of these hydrogels with synthetic oxygen carriers, like perfluorocarbons (PFC), leads to increased stem cell survival and enhanced bone formation in vivo[4].

The hypothesis of this study is that the minimally invasive injection of MSCs with a biocompatible scaffold, into the vertebral body will regenerate the spinal vertebral body and accelerate bone repair.

Specific Aims:

- Inducing bone regeneration of a vertebral defect in a rat model by implantation of porcine adipose derived MSCs.
- Monitoring cell survival and bone formation kinetics based on optical (bioluminescence and fluorescence) molecular and micro imaging.
- Determine optimal cell scaffold compositions that would yield the desired osteogenic effect.

***Methods*:**

In order to induce osteogenic differentiation of the porcine adipose derived MSCs, and to promote bone formation in vivo, the cells will be transfected with an osteogenic gene, BMP-6,

using a non-viral method based on electroporation. We have previously shown that robust bone formation can be induced when BMP-6 electroporated porcine MSCs were implanted in vivo in mice[31] (Fig. 4.2). This is a safe method that overcomes the disadvantages of using viral gene delivery techniques. In addition, in order to allow for stem cell tracking and monitoring of survival in vivo, the cells will be infected with lenti and retroviruses encoding for luciferase and GFP marker genes (at multiplicity of infection [MOI] of 100). Different combinations of hydrogels, PFCs and MSCs will be tested to determine, which the most potent bone-inductive combination. Testing will include ectopic implantations in NOD/SCID mice followed by quantification of bone formation and cell survival using micro CT and bioluminescence imaging (Fig. 4.3). A rat model of critical-size vertebral bone defect will be used to test the capability of engineered MSCs to regenerate bone. We have already established this model in a rat by drilling a 1x3mm cylindrical defect in the coccygeal vertebra (Fig. 4.4). Injections of engineered MSCs will be made into nude rat (female, 10-12 weeks of age, weighing 120-180 gram) coccygeal vertebra (Levels C3). A volume of 20 µl, containing cells in selected hydrogel gel at a density of 1x106 cells/ml, will be injected. Cell survival will be monitored using bioluminescence (IVIS Lumina Optical, Xenogen; Fig. 4.1 b and 4.3 d). For bioluminescence imaging, rats will be injected with Luciferin. Cell survival will be monitored up to eight weeks post MSC injection. The in vivo results measurements of cell survival will be validated by an invasive method in which the implants will be excised and GFP-labeled cells will be counted by flow cytometry. The extent of bone formation and defect repair will be measured using periodic scans with micro CT (Fig. 4.4 c, d). Finally, the biodistribution of the implanted cells will be validated as well by harvesting blood, brain, spleen, kidney, heart, lung, liver and thigh muscles from rats. DNA will be extracted and followed by quantitative PCR using specific primers for the Luciferase transgene (ABI Prism System, Applied Biosystems).

***Preliminary results*:**

In addition to our published work, new unpublished preliminary data that provide direct support to studies proposed in this chapter have been acquired. These are summarized in the accompanying figures.

Survival of MSCs After Injection into Rat Intervertebral Discs: We first performed imaging studies to establish methods to image MSC survival in vivo using fluorescence and bioluminescence, both of which are proposed in this chapter. Figure 4.1 shows in vivo fluorescent and bioluminescent imaging of MSC survival. Engineered MSCs overexpressing BMP-2 under tetracycline regulation (tet-off) were injected into tail intervertebral discs of nude rats under fluoroscopic guidance (Fig. 4.1 a). Since the cells were infected with GFP and luciferase marker

genes prior to the injection, we were able to monitor the cell survival within the disc using bioluminescent and fluorescent imaging. Luciferase expression was detected using a bioluminescence imaging system (Fig. 4.1 b) and the GFP signal was detected (Fig. 4.1 c) using a fibered fluorescent imaging system (CellVizio, MaunaKea Tech, France).

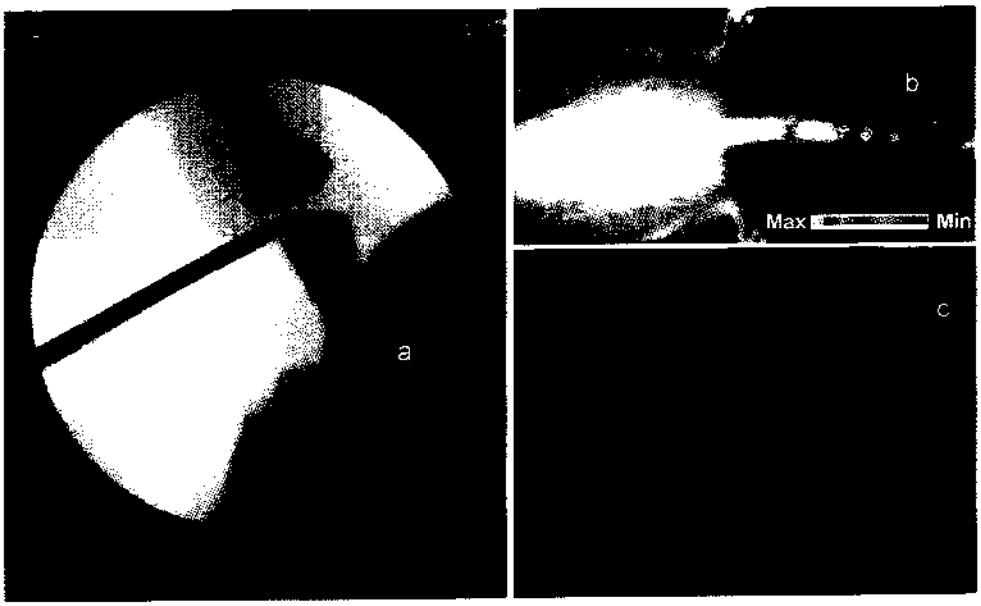

Figure 4.1: In vivo fluorescent and bioluminescent imaging of MSCs survival (a – c).

Adipose Derived MSC-Based Spine Fusion: Porcine MSCs were isolated from pig subcutaneous adipose tissue and expanded in culture as described by Zuk et al., 2001 [50]. The cells were nucleofected with a hBMP-6 encoding plasmid as we have described for human MSCs [49]. 24 hours post transfection 5x106 nucleofected cells were mixed with fibrin gel (Tisseel TM kit, Baxter AG, Vienna, Austria) and injected into the right para-spinal muscle of the lumbar spine of NOD/SCID mice (n = 5). In vivo, bone formation was monitored in real time, using a non-invasive fluoroscan

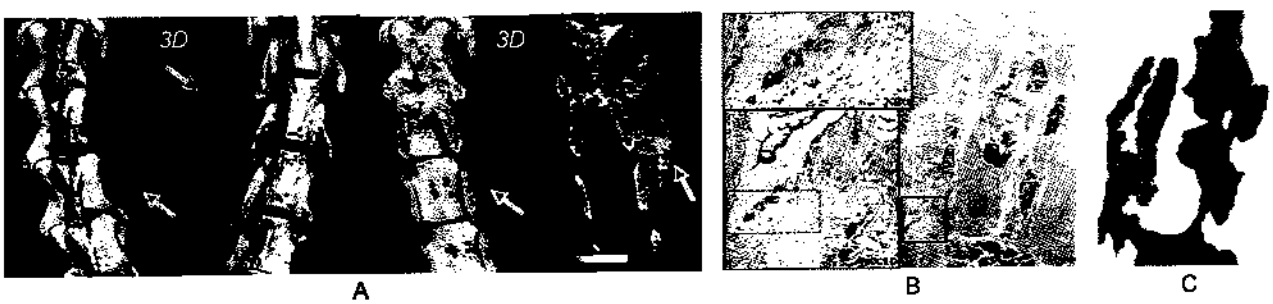

Figure 4.2: Genetically modified porcine adipose tissue-derived stem cells (MSCs) induced spinal fusion in vivo. μCT scan (A). The new bone formation was contoured manually and depicted in orange color on the 3D reconstructed images. Representative lateral view of 3D image of fused spine on left side and coronal sections in 2D and 3D on the right. Histological analysis using standard H&E stain (B) and schematic map of the histological sections (C) in which green - fusion bone mass, red - bone marrow and blue - intact vertebrae.

device and a quantitative micro computerized tomography system (μCT40, Scanco, Switzerland) (Fig. 4.2 A). Bone formation was also evaluated using Hematoxylin and Eosin (H&E) and Mason Tri Chrome stained histological sections (Fig. 4.2 B, C).

Oxygen Supplementation Enhances Ectopic Bone Formation: The following preliminary results show that engineered stem cells demonstrated higher survival rate and generated larger amount of bone tissue in vivo when suspended in hydrogels enriched with perfluorocarbon molecules. We have prepared Fibrin hydrogels enriched with 5 or 10% perfluorotributylamine (PFTBA, Sigma) in which $3x10^6$ tet-off BMP-2 stem cells were suspended. The cell-fibrin mixture was then injected subcutaneously to C3H/HeN mice. Since the cells were also expressing the Luciferase marker gene, we could detect cell survival using a bioluminescence imaging system. Our results indicated that bone volume was significantly increased in the PFTBA groups two weeks post injection as demonstrated by quantitative micro-CT (Fig. 4.3 A, B). Moreover, bone formation was accelerated in the PFTBA groups, since on Day 7 bone trabecules were already evident in the 10% PFTBA group, compared to the NO PFTBA control that showed only proliferative cartilage (Fig.4.3 C). Furthermore, an increase in cell survival was noticed on Day 3 and 7 in the 10%PFTBA group compared to the No PFTBA group, based on the detected luciferase signal (Fig. 4.3 D).

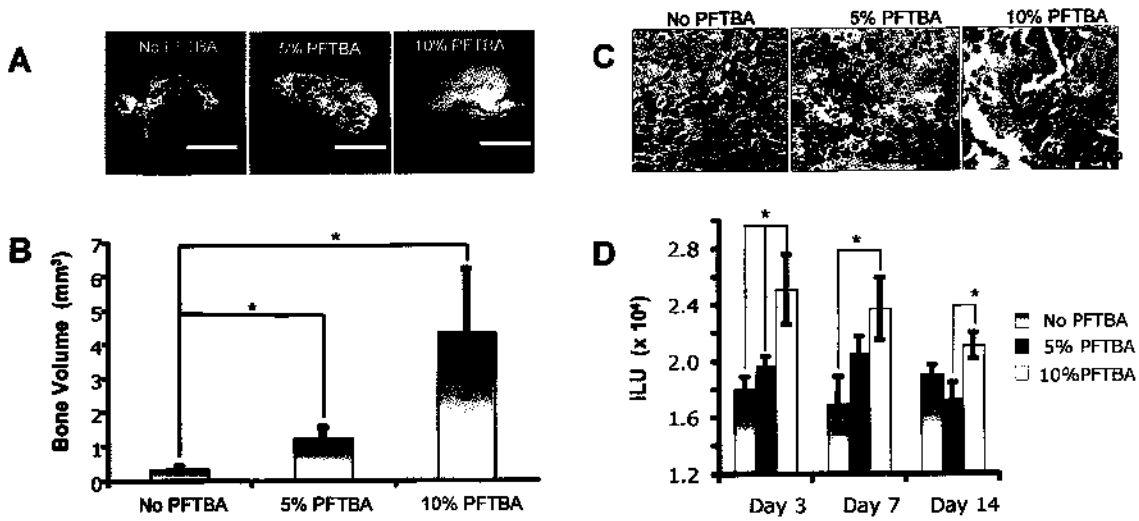

Figure 4.3: **The influence of PFTBA-enriched hydrogel on stem cell survival and bone formation in vivo. Bone formation was analyzed two weeks post injection using μCT scans: (a): 3D images of the ectopic bone formed subcutaneously. (b) Quantitative analysis of the micro-CT data showed the higher bone volume was formed in the group injected with 10% PFTBA. (c): Masson's Trichrome staining of the implants of BMP-2 engineered MSCs, on Day 7 post-implantation. Note that bone trabeculae are already identified in the 10% PFTBA group while in hydrogels without PFTBA, only proliferative cartilage is seen. (d) Quantitative analysis of the Luciferase signal (in integrated light units, ILU) demonstrated that the signal was significantly higher in the group implanted with 10% PFTBA on Day 3 and 7 post injection (n=3; $p<0.05$).**

Vertebral Fracture Model in a Rat: Bone void defect was created in Nude rat-tail vertebra by drilling a 1 x 3mm cylindrical defect in the coccygeal vertebra. Porcine MSCs were nucleofected with BMP6 and the cells were injected with fibrin gel into the bone void. The repair process was monitored in vivo using fluoroscan (Fig. 4.4 A, B) μCT in vivo (Fig. 4.4 C) and in vitro (Fig. 4.4 d). The scans on day 0 (Fig. 4.4 A) showed a vast defect in the vertebra. μCT scan in vivo (Fig. 4.4 C), 8 weeks after the operation, showed noticeable radiolucent area at the defect site. Three months after the operation fluoroscope and μCT in vitro scans showed almost complete repair of the vertebral defect (Fig. 4.4 B, D).

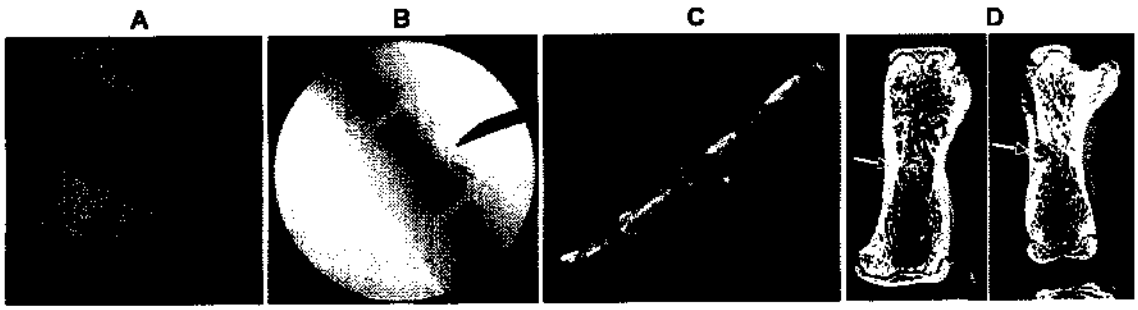

Figure 4.4: Rat coccyges vertebral defect transplanted with porcine MSCs nucleofected with BMP6. Bone void defects were created in nude rat-tail vertebrae. Porcine MSCs were nucleofected with BMP6 and the cells were injected in fibrin gel into the bone void. The repair process was monitored in vivo using fluoroscan (A, B) and μCT in vivo (C) and in vitro (D). The scans on day 0 (A) showed vast defect inside the vertebra. μCT scan in vivo (c) 8 weeks after the operation showed a noticeable radiolucent area at the defect site. Three months after the operation fluoroscope and μCT in vitro scans showed almost complete repair of the vertebral defect (B, D).

Discussion and future plans:

The objective of this study is to monitor stem cell-based vertebral fracture repair using molecular and tissue imaging modalities. The preliminary results show that utilizing genetically engineered porcine adipose derived MSCs with a biocompatible scaffold, for implantation into a fractured vertebral body of a rat model, can be monitored for cell survival and bone formation kinetics based on optical (bioluminescence and fluorescence) molecular and micro imaging.

Further investigations will include: (as detailed in the specific aims and methods sections)

- *Implantation of adipose derived porcine MSCs in the rat model to induce bone regeneration.*
- *Monitoring cell survival and bone formation kinetics using optical imaging (bioluminescence and fluorescence) and micro CT.*
- *Determining optimal cell-scaffold compositions that produce the desired osteogenic effect.*

References:

1. Kimelman, N., Pelled, G., Gazit, Z. & Gazit, D. Applications of gene therapy and adult stem cells in bone bioengineering. Regenerative Medicine 1, 549-561 (2006).
2. Holdsworth, D. W. & Thornton, M. M. Micro-CT in small animal and specimen imaging. Trends in Biotechnology 20, S34-S39 (2002).
3. Hildebrand, T., Laib, A., Muller, R., Dequeker, J. & Ruegsegger, P. Direct three-dimensional morphometric analysis of human cancellous bone: microstructural data from spine, femur, iliac crest, and calcaneus. J Bone Miner Res 14, 1167-74 (1999).
4. Kimelman-Bleich, N. et al. The use of a synthetic oxygen carrier-enriched hydrogel to enhance mesenchymal stem cell-based bone formation in vivo. Biomaterials 30, 4639-48 (2009).
5. Tai, K. et al. Nanobiomechanics of repair bone regenerated by genetically modified mesenchymal stem cells. Tissue Eng Part A 14, 1709-20 (2008).
6. Steinhardt, Y. et al. Maxillofacial-derived stem cells regenerate critical mandibular bone defect. Tissue Eng Part A 14, 1763-73 (2008).
7. Ntziachristos, V., Ripoll, J., Wang, L. V. & Weissleder, R. Looking and listening to light: the evolution of whole-body photonic imaging. Nat Biotechnol 23, 313-20 (2005).
8. Graves, E. E., Ripoll, J., Weissleder, R. & Ntziachristos, V. A submillimeter resolution fluorescence molecular imaging system for small animal imaging. Med Phys 30, 901-11 (2003).
9. Montet, X., Ntziachristos, V., Grimm, J. & Weissleder, R. Tomographic fluorescence mapping of tumor targets. Cancer Res 65, 6330-6 (2005).
10. Zaheer, A. et al. In vivo near-infrared fluorescence imaging of osteoblastic activity. Nat Biotechnol 19, 1148-54 (2001).
11. Gazit, D. et al. Engineered pluripotent mesenchymal cells integrate and differentiate in regenerating bone: a novel cell-mediated gene therapy. J Gene Med 1, 121-33 (1999).
12. Moutsatsos, I. K. et al. Exogenously regulated stem cell-mediated gene therapy for bone regeneration. Mol Ther 3, 449-61 (2001).
13. Wozney, J. M. et al. Novel regulators of bone formation: molecular clones and activities. Science 242, 1528-34 (1988).
14. Wang, E. A. et al. Recombinant human bone morphogenetic protein induces bone formation. Proc Natl Acad Sci U S A 87, 2220-4 (1990).
15. Volek-Smith, H. & Urist, M. R. Recombinant human bone morphogenetic protein (rhBMP) induced heterotopic bone development in vivo and in vitro. Proc Soc Exp Biol Med 211, 265-72 (1996).
16. Katagiri, T. et al. The non-osteogenic mouse pluripotent cell line, C3H10T1/2, is induced to differentiate into osteoblastic cells by recombinant human bone morphogenetic protein-2. Biochem Biophys Res Commun 172, 295-9 (1990).
17. Chen, P., Carrington, J. L., Hammonds, R. G. & Reddi, A. H. Stimulation of chondrogenesis in limb bud mesoderm cells by recombinant human bone morphogenetic protein 2B (BMP-2B) and modulation by transforming growth factor beta 1 and beta 2. Exp Cell Res 195, 509-15 (1991).
18. Thies, R. S. et al. Recombinant human bone morphogenetic protein-2 induces osteoblastic differentiation in W-20-17 stromal cells. Endocrinology 130, 1318-24 (1992).
19. Wang, E. A., Israel, D. I., Kelly, S. & Luxenberg, D. P. Bone morphogenetic protein-2 causes commitment and differentiation in C3H10T1/2 and 3T3 cells. Growth Factors 9, 57-71 (1993).

20. Rosen, V. et al. Responsiveness of clonal limb bud cell lines to bone morphogenetic protein 2 reveals a sequential relationship between cartilage and bone cell phenotypes. J Bone Miner Res 9, 1759-68 (1994).

21. Yamaguchi, A. Regulation of differentiation pathway of skeletal mesenchymal cells in cell lines by transforming growth factor-beta superfamily. Semin Cell Biol 6, 165-73 (1995).

22. Yamaguchi, A. et al. Effects of BMP-2, BMP-4, and BMP-6 on osteoblastic differentiation of bone marrow-derived stromal cell lines, ST2 and MC3T3-G2/PA6. Biochem Biophys Res Commun 220, 366-71 (1996).

23. Chaudhari, A., Ron, E. & Rethman, M. P. Recombinant human bone morphogenetic protein-2 stimulates differentiation in primary cultures of fetal rat calvarial osteoblasts. Mol Cell Biochem 167, 31-9 (1997).

24. Hay, E., Hott, M., Graulet, A. M., Lomri, A. & Marie, P. J. Effects of bone morphogenetic protein-2 on human neonatal calvaria cell differentiation. J Cell Biochem 72, 81-93 (1999).

25. Ahrens, M. et al. Expression of human bone morphogenetic proteins-2 or -4 in murine mesenchymal progenitor C3H10T1/2 cells induces differentiation into distinct mesenchymal cell lineages. DNA Cell Biol 12, 871-80 (1993).

26. Lou, J., Xu, F., Merkel, K. & Manske, P. Gene therapy: adenovirus-mediated human bone morphogenetic protein-2 gene transfer induces mesenchymal progenitor cell proliferation and differentiation in vitro and bone formation in vivo. J Orthop Res 17, 43-50 (1999).

27. Turgeman, G. et al. Engineered human mesenchymal stem cells: a novel platform for skeletal cell mediated gene therapy. J Gene Med 3, 240-51 (2001).

28. Zilberman, Y. et al. Fluorescence molecular tomography enables in vivo visualization and quantification of nonunion fracture repair induced by genetically engineered mesenchymal stem cells. J Orthop Res 26, 522-30 (2008).

29. Kimelman, N. et al. Review: gene- and stem cell-based therapeutics for bone regeneration and repair. Tissue Eng 13, 1135-50 (2007).

30. Hasharoni, A. et al. Murine spinal fusion induced by engineered mesenchymal stem cells that conditionally express bone morphogenetic protein-2. J Neurosurg Spine 3, 47-52 (2005).

31. Sheyn, D. et al. Nonvirally engineered porcine adipose tissue-derived stem cells: use in posterior spinal fusion. Stem Cells 26, 1056-64 (2008).

32. Jamsa, T., Jalovaara, P., Peng, Z., Vaananen, H. K. & Tuukkanen, J. Comparison of three-point bending test and peripheral quantitative computed tomography analysis in the evaluation of the strength of mouse femur and tibia. Bone 23, 155-61 (1998).

33. Keaveny, T. M., Pinilla, T. P., Crawford, R. P., Kopperdahl, D. L. & Lou, A. Systematic and random errors in compression testing of trabecular bone. J Orthop Res 15, 101-10 (1997).

34. Odgaard, A. & Linde, F. The underestimation of Young's modulus in compressive testing of cancellous bone specimens. Journal of Biomechanics 24, 691-8 (1991).

35. Yang, G. et al. The anisotropic Hooke's law for cancellous bone and wood. J Elast 53, 125-46 (1998).

36. Ladd, A. J., Kinney, J. H., Haupt, D. L. & Goldstein, S. A. Finite-element modeling of trabecular bone: comparison with mechanical testing and determination of tissue modulus. J Orthop Res 16, 622-8 (1998).

37. van Rietbergen, B., Weinans, H., Huiskes, R. & Odgaard, A. A new method to determine trabecular bone elastic properties and loading using micromechanical finite-element models. J Biomech 28, 69-81 (1995).

38. Kallai, I. et al. Quantitative, structural, and image-based mechanical analysis of nonunion fracture repaired by genetically engineered mesenchymal stem cells. J Biomech In Press (2010).

39. Parfitt, A. M. Implications of architecture for the pathogenesis and prevention of vertebral fracture. Bone 13 Suppl 2, S41-7 (1992).

40. Oner, F. C., Verlaan, J. J., Verbout, A. J. & Dhert, W. J. Cement augmentation techniques in traumatic thoracolumbar spine fractures. Spine 31, S89-95; discussion S104 (2006).

41. De Negri, P., Tirri, T., Paternoster, G. & Modano, P. Treatment of painful osteoporotic or traumatic vertebral compression fractures by percutaneous vertebral augmentation procedures: a nonrandomized comparison between vertebroplasty and kyphoplasty. Clin J Pain 23, 425-30 (2007).

42. Black, D. M. et al. Randomised trial of effect of alendronate on risk of fracture in women with existing vertebral fractures. Fracture Intervention Trial Research Group. Lancet 348, 1535-41 (1996).

43. Greenspan SL et al. Effect of recombinant human parathyroid hormone (1-84) on vertebral fracture and bone mineral density in postmenopausal women with osteoporosis: a randomized trial. Ann Intern Med. 146, 326-39 (2007).

44. Furtado, N., Oakland, R. J., Wilcox, R. K. & Hall, R. M. A biomechanical investigation of vertebroplasty in osteoporotic compression fractures and in prophylactic vertebral reinforcement. Spine 32, E480-7 (2007).

45. Bonardel, G. et al. Pulmonary cement embolism after percutaneous vertebroplasty: a rare and nonthrombotic cause of pulmonary embolism. Clin Nucl Med 32, 603-6 (2007).

46. Duran, C. et al. Pulmonary cement embolism: a complication of percutaneous vertebroplasty. Acta Radiol 48, 854-9 (2007).

47. Lim, S. H., Kim, H., Kim, H. K. & Baek, M. J. Multiple cardiac perforations and pulmonary embolism caused by cement leakage after percutaneous vertebroplasty. Eur J Cardiothorac Surg 33, 510-2 (2008).

48. Son, K. H., Chung, J. H., Sun, K. & Son, H. S. Cardiac perforation and tricuspid regurgitation as a complication of percutaneous vertebroplasty. Eur J Cardiothorac Surg 33, 508-9 (2008).

49. Aslan, H. et al. Nucleofection-based ex vivo nonviral gene delivery to human stem cells as a platform for tissue regeneration. Tissue Eng 12, 877-89 (2006).

50. Zuk, P. A. et al. Multilineage cells from human adipose tissue: implications for cell-based therapies. Tissue Eng 7, 211-28 (2001).